Arab J Geosci (2017) 10: 476
https://doi.org/10.1007/s12517-017-3253-0

GEOMEAST2017

# Finite element analysis of the propagation of Earth's surface deformation as a consequence of normal dip-slip offshore fault rupture

Lama Thebian[1] · Salah Sadek[1] · Shadi Najjar[1] · Mounir Mabsout[1]

Received: 31 July 2017 / Accepted: 23 October 2017 / Published online: 13 November 2017


**Abstract** This paper addresses the deformation response of seabed sands subject to underlying normal fault movement. This problem is relevant to the design of overlying offshore structures and subsea oil/gas pipelines connecting offshore platforms to the shoreline. The mechanism of the fault propagation in overlying seabed deposits is examined using 2D finite element modeling. Abaqus© is used as a numerical platform in modeling this complex problem, while accounting for nonlinear soil behavior with strain softening. Different dip angles and vertical fault displacements of up to 10% of the soil layer thickness were considered. The results include the effect of the relative density of the seabed sands and the soil layer thickness on the extent and magnitude of ground surface deformations. The required bedrock displacement/offset for the rupture to reach the surface and the length and location of the distorted zone are also investigated. Based on the parametric analyses and results presented in this paper, observations related to the potential magnitudes and extents of surface deformations for various conditions of seabed densities and thicknesses are provided. These would be of importance in determining likely effects of distortion/loading on pipelines and offshore structures crossing the fault zone.

**Keywords** Normal faulting · Offshore geotechnics · Finite element analyses

This article is part of the Topical Collection on *Geotechnical Engineering for Urban and Major Infrastructure Development*

✉ Lama Thebian
ltt00@aub.edu.lb

Salah Sadek
salah@aub.edu.lb

Shadi Najjar
sn06@aub.edu.lb

Mounir Mabsout
mounir@aub.edu.lb

[1] Department of Civil & Environmental Engineering, American University of Beirut, P.O. Box 11-0236, Riad El-Solh, Beirut 1107-2020, Lebanon

## Introduction

Historically, earthquakes that were triggered by dip-slip fault systems (normal or reverse) have caused significant damage to structures, human lives, and the environment. Specific examples of cases of normal faults include the Manhattan earthquake (1867), Atalanti earthquake (1894), L'Aquila earthquake (2009), Hamadori earthquake (2011), and Norcia earthquake (2016) among many others. Damage of onshore oil and gas facilities by normal faults could lead to large economical losses due to service shut down, business interruption, property losses, and replacement costs. A notable example is the damage suffered by the largest refinery in Korfez, Turkey as a result of the 1999 Kocaeli earthquake (Bendimerad et al. 2000). Despite the significant knowledge garnered over the years in reference to offshore pipelines, the understanding of their response when subjected to permanent ground deformations resulting from the propagation of the fault movement through seabed deposits is still insufficient. This is in part due to the fact that most of the well documented offshore projects have been constructed in non-seismic zones, e.g., the North Sea, Western Australia, and the Gulf of Mexico. As such, there is a clear need for efforts aimed at investigating the mechanism of fault movement propagation through overlying soil deposits, in order to quantify the extent and magnitude of the strain and stress fields, which will affect pipelines resting on, or buried within, the seabed deposits.

The risk of offshore pipelines crossing faults is relevant and potentially critical in several locations in the world. One specific example is the case of the Eastern Mediterranean where oil and gas reserves have been proven and where only recently have efforts at actual exploitation and extraction been initiated. Another example of such geo-risks is that of the Japan-Sakhalin Gas Pipeline which intersects an active normal fault offshore Chiba prefecture, to the east of Tokyo (Trimintziou et al. 2015). Likewise, subsea pipelines potentially vulnerable to active normal faulting are located in the Euboean Gulf in Greece and in the Caspian Sea.

Normal faults are classified as “low-angle” normal faults or lags (Park et al. 2013) when their dip angles are less than 45°, otherwise they are characterized as “high-angle” normal faults. Cases of shallow normal faults are the Gulf of Corinth (Rietbrock et al. 1996) and Papua New Guinea (Abers 1991). Limited research was done to investigate the propagation of low-angle normal faults in subsea sediments in relation to pipeline design and stability. The possibility that offshore pipelines could cross active normal fault zones necessitates special design considerations to ensure the safety and stability of these systems. Several research studies targeted this problem using experimental programs. Sanford (1959), Belousov (1961), Emmons (1969), Horsfield (1977), Cole and Lade (1984), Lade et al. (1984), Bray et al. (1993), and Johansson and Konagai (2004) conducted 1-g small scale experiments, while Bransby et al. (2008a, 2008b) used centrifuge experiments to model dip-slip fault propagation. Other researchers approached the problem using numerical modeling and analysis methods. Scott and Schoustra (1974) simulated vertical fault propagation through a 800 m deep, dry, cohesionless alluvium using numerical analysis. Roth et al. (1982), Scott (1987), White et al. (1994), Nakai et al. (1995), Loukidis (1999), and Loukidis et al. (2009) used the finite difference method to tackle similar problmes. Bray et al. (1994), Taniyama and Watanabe (2002), and Lin et al. (2006), and Anastasopoulos et al. (2007) conducted experiments coupled with finite element models.

The present paper extends previous research on fault propagation which was limited to one relative density (Johanson and Konagai 2007), low bedrock displacements (Loukidis et al. 2009), onshore cases (Anastasopoulos et al. (2007), and steep dip angles, to include the effect of various sand relative densities (20, 50, and 80%), dip angles (15°, 30°, 45°, 60°, and 75°), and fault displacements as large as 10% of the thickness of the soil layer overlying the faulted rock. The effect of different soil layer thicknesses ($H$ = 10, 20, 40, and 80 m) is also assessed. The offshore fault propagation problem is realistically investigated through a numerical finite element analysis that accurately depicts the geometry, boundary conditions, and soil properties, while ensuring that the proper effective stress state is considered. It is worth noting that hidden faults are not studied in this article.

## Numerical modeling

The displacement response of offshore sands that overly normal faults is analyzed numerically using the advanced computational tool Abaqus v.6.13. The adopted model simulates the behavior of the saturated sand using effective stress analysis by considering eight node plain strain quadrilateral, biquadratic displacement, bilinear pore elements (CPE8P) assuming quasi-static loading. Drained conditions are assumed for the sand, and a density of 1120 Kg/m$^3$ is considered for the seawater. It is worth noting that given drained conditions, the depth of the seawater does not influence the effective stresses and the numerical results.

### Model geometry, mesh, and boundary conditions

A 2D plain strain model of dimensions 20 m × 140 m is adopted to simulate the normal fault propagation mechanism in the offshore sand sediments overlying a “seismic substratum” or rocky ground. The theoretical model is shown in Fig. 1 and illustrates the (1) overlying soil layer (thickness $H$ = 20 m as a base case), (2) applied fault displacement, and (3) adopted finite element mesh. In the zone near the fault where the fault rupture and large deformations prevail, the mesh is comprised of 0.5 m × 0.5 m quadratic elements. The mesh becomes coarser in the zone that is further away from the fault. The following steps have been adopted in the simulation: (1) application of the self-weight and water load and (2) application of fault displacement by subjecting the external nodes of the moving part to displacement-controlled loading in the direction of a pre-set dip-angle. To cater for discontinuity and convergence problems, the fault displacement was applied within a width of 1 m. At any displacement increment, a linearly-varying fault movement is forced along this 1-m width, by fixing the right end of this width and moving the left end in accordance with the applied fault displacement.

### Soil constitutive model and properties

Relevant material characteristics used in our analyses are presented in Table 1. Elastoplastic material behavior that is based on a modified Mohr-Coulomb model that is capable of modeling strain softening is used to model the sand behavior. The strain-softening response was modeled by

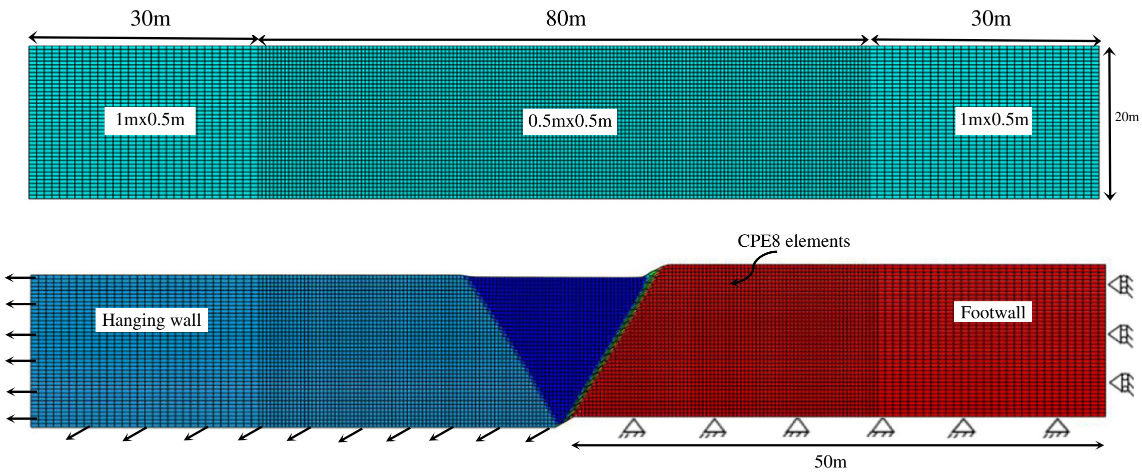


**Fig. 1** The **a** un-deformed and **b** deformed shape of the 2D finite element model showing dimensions and mesh size

reducing the peak friction and dilation angles as a function of the deviatoric plastic strain such that:

$$\Phi_{\text{mob}} = \begin{cases} \Phi_p - \dfrac{\Phi_p - \Phi_{\text{cr}}}{\gamma^f_{\text{dev}}}\gamma^p_{\text{dev}} & for \quad 0 \le \gamma^p_{\text{dev}} \le \gamma^f_{\text{dev}} \\ \Phi_{\text{res}} & for \quad \gamma^p_{\text{dev}} \ge \gamma^f_{\text{dev}} \end{cases} \tag{1}$$

$$\Psi_{\text{mob}} = \begin{cases} \Psi_p\left(1 - \dfrac{\gamma^p_{\text{dev}}}{\gamma^f_{\text{dev}}}\right) & for \quad 0 \le \gamma^p_{\text{dev}} \le \gamma^f_{\text{dev}} \\ \Psi_p & for \quad \gamma^p_{\text{dev}} \ge \gamma^f_{\text{dev}} \end{cases} \tag{2}$$

Sands with three relative densities (20, 50, and 80%) were considered in the analysis to represent loose, medium dense, and dense sands, respectively. Round-shaped, uniform, medium sand with a coefficient of uniformity $C_u = 3$, and a typical specific gravity of $G_s = 2.67$ was adopted. The maximum and minimum void ratios were estimated as a function of the relative densities based on Youd et al. (1973) as per the EPRI design manual (Kulhawy and Mayne 1990). The stiffness and shear strength properties as reflected in the modulus of elasticity ($E$), the peak friction angle ($\Phi_{\text{peak}}$), the peak dilation angle ($\Psi_{\text{peak}}$), and the Poisson's ratio ($\upsilon$) of the three sand classes vary with increasing confining pressure and therefore with depth ($z$) as indicated in Table 1.

Typical values of $E_0$ of 15,600, 22,000, and 33,000 KPa were assumed at the surface, and the stiffness was increased with depth based on Schanz and Vermeer (1998). Schanz and Vermeer (1998) noted that the exponent $m$ in eq. (3) attains values ranging between 0.4 and 0.75 based on oedometer and triaxial tests for different sands compared with previous researchers. So, a typical value of 0.5 was assumed for the exponent m in this article. In equation 3, $\sigma_v$ represents the vertical stress and $\sigma_a$ stands for the atmospheric pressure.

$$E = E_0\left(\frac{\sigma'_v}{\sigma_a}\right)^m \tag{3}$$

The critical friction angle was assumed equal to 30° based on Koerner (1970). The peak friction angle ($\phi_p$) was

**Table 1** Shear strength properties of the saturated dense, medium dense, and loose sand

| Density | Dense | Medium dense | Loose |
|---|---|---|---|
| RD | 80% | 50% | 20% |
| $K_0$ | 0.35 | 0.42 | 0.5 |
| $E$ (KPa) | $11209\sqrt{z}$ | $7300\sqrt{z}$ | $5063\sqrt{z}$ |
| $C$ (KPa) | 2 | 2 | 2 |
| $\Phi_p$(°) | $51 - 2.4\ln(6.85z) \le 42$ | $42 - 1.5\ln(6.9z)$ | 30 |
| $\Phi_{\text{res}}$ (°) | 30 | 30 | 30 |
| $\nu$ | $0.49 - 0.036\ln(6.85z)$ | $0.355 - 0.0225\ln(6.9z)$ | 0.18 |
| $\Psi_p$ (°) | $26.25 - 3\ln(6.85z)$ | $15 - 1.88\ln(6.9z)$ | 0 |
| $\Psi_{\text{res}}$(°) | 0.1 | 0.1 | 0.1 |
| $\gamma^p_f$ | 0.1 | 0.1 | – |

calculated from Bolton (1986) as $\phi_{peak} - \phi_{cr} = 3(D_r[10 - \ln(100P_f/P_a)] - 1)$. It is worth noting that the upper bound of the peak friction angle was taken as 42°. The dilation angle ($\Psi$) was estimated from Bolton's (1986) equation as $\Psi\text{peak} = (\phi_{peak} - \phi_{cr})/0.8$. Poisson's ratio was estimated based on EPRI (Kulhawy and Mayne 1990) as $\upsilon_d = 0.1 + 0.3\phi_{rel}$ where $\phi_{rel} = (\phi_{peak}–25)/(45−25)$.

## Numerical results

In Section 3.1, a model with a height of 20 m and length of 140 m is analyzed. As a base case, finite element analyses were performed for a dense sand layer subjected to a normal fault having a dip angle of 45°. The relative density of the sand was then varied to include medium-dense and loose cases in Section 3.2. In Section 3.3, the results of the base case model were compared with cases where the dip angle of the normal fault was considered to be 15°, 30°, 60°, and 75° to assess the effect of the fault dip angle on the propagation mechanism. The combined effect of relative density and fault dip angle is then studied in Section 3.4. Finally, in Section 3.5, the height of the overlying soil layer is varied from $H = 20$ to $H = 10$, 40, and 80 m to investigate the influence of the sand layer thickness on the fault propagation mechanism. In all the analyses, vertical bedrock displacements ($U$) up to 10% of the soil layer thickness are enforced. The results include an analysis of the vertical ground surface deformation profile ($y$), the horizontal distance ($S$) from the location of the shear band to the center of the fault ($O$) (see Fig. 6), the critical inclined bedrock displacement required for the shear band to reach the surface ($d_{crit}$), the length ($L$), and center ($C$) of the distorted zone. In the results section, most of the predefined parameters are normalized with the soil layer thickness $H$.

### The base-case model ($H$ = 20 m, dense sand, and $\alpha$ = 45°)

Figure 2 shows the deformed shape of the finite element model describing a dense sand layer of thickness $H$ = 20 m subjected to a normal fault of dip angle 45° at a vertical bedrock displacement of $U$ = 10%H. The deformed shape indicates the formation of primary and secondary shear surfaces within the sand layer as a result of the normal fault movement in the underlying bedrock. The primary shear plane propagates within the footwall block while the secondary shear band forms within the hanging wall, resulting in the formation of a graben structure having an inverted triangular shape. The formation of grabens in normal faults has been reported in several published experimental and numerical studies (Anastasopoulos et al. 2007; Loukidis et al. 2009; and Nollet et al. 2012).

Normalized ground surface deformation profiles depicting the variation of the normalized vertical ground surface deformations ($y/H$) along the model width are presented in Fig. 3 for vertical bedrock displacements ranging from 0.5 to 10% of the soil layer thickness ($H$). These surface deformation profiles provide essential input for mitigating the fault rupture geohazard which requires accounting for fault-induced ground surface deformations (Kelson et al. 2001 and Chang et al. 2015). At a low bedrock displacement of 0.5%H, the hanging wall is displaced in the direction of the dip angle, and a primary shear band forms and propagates to the surface forming a scarp of height $s_f \approx 0.5\ \%$ H. At $U$ = 1%H, a secondary shear band forms and propagates to the surface inducing the formation of a graben structure as a second scarp appears on the hanging wall. At this stage, the length of the graben is approximately $L_g = 1.2$H and the graben scarp height is $s_g = 0.05\ \%\ H$. Subsequently, with increasing bedrock displacement, the graben displaces in the downward direction and its height increases to a value of $s_g$= 2.3%H and its length to $L_g$ = 1.45H at U = 10%H.

#### *Extent and location of the shear surface/band*

The mechanism in which the shear band forms and propagates to the surface is illustrated in Fig. 4. As the hanging wall is moved in the dip angle direction, shearing occurs between the footwall and the hanging wall, and the earliest signs of a shear band are observed at a vertical fault displacement as small as 1 cm (Fig. 4a). With additional fault displacement, a fully developed primary shear band with a spiral shape is observed as the fault propagates to the surface at vertical displacements ranging from 1.4 to 1.5 cm (Fig. 4 b, c). The horizontal distance from the center of the fault to the location of the primary shear surface/band could be estimated to be around $S$ = 0.59H. With increasing bedrock displacement, large deformations are induced, and the shape of the shear band transforms from spiral to straight (Fig. 4d). These results indicate the significance of understanding the fault propagation mechanism and its impact on the resulting surface deformations which could affect the design of overlying structures.

Based on the results of the base case model, it could be concluded that the primary shear band reaches the ground

**Fig. 2** The deformed shape of the reference model (dense sand, dip angle = 45°, soil layer thickness $H$ = 20 m)

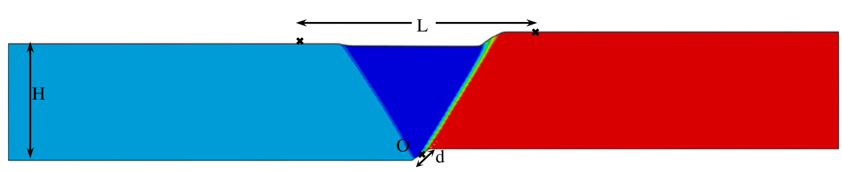

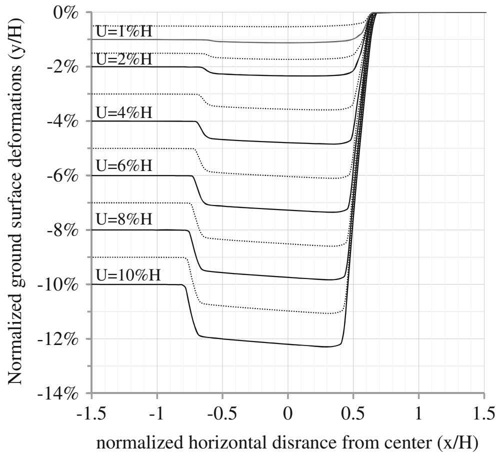


**Fig. 3** Normalized ground surface deformation profile ($y/H$) of the reference model (dense sand, dip angle = 45°, soil layer thickness $H$ = 20 m) for vertical bedrock displacements ranging from $U$ = 1%H to $U$ = 10%H)

level at an inclined bedrock fault displacement in the order of 0.085%H (at a vertical bedrock displacement of 0.012 m). This critical bedrock displacement $d_{crit}$ will be referred to as the critical fault displacement in the balance of this paper. The criterion adopted to determine $d_{crit}$ is the instance at which the yield points of the primary shear band reach the ground surface level. Upon fault rupture and depending on the magnitude of the fault displacement, the shear band could propagate to the surface resulting in risk of potential damage to overlying structures (Chang et al. 2015). Since the critical bedrock displacement $d_{crit}$ is expected to be a function of the thickness of the sand cover, its accurate determination for any given offshore project will be highly dependent on the reliability of the site investigation and the variability in the depth and thickness of the sand cover layer above the basement fault.

*Length and center of distorted zone*

Prior to propagating to the top surface, the shear strains in the overlying sand layer may lead to distortion of the soil medium and increasing inclinations in the ground surface. In the zone affected by the fault propagation, the soil is expected to suffer from softening and strength loss, compromising the stability or serviceability of any structure (ex. pipeline) that is supported on the soil. Therefore, a proper delineation of the distorted zone that is affected by the fault propagation mechanism is essential to locate the lateral extent of zones that would ensure minimal interference with the fault propagation mechanism. The distorted zone ($L$) was defined by Loukidis et al. (2009) as the length of the zone within which the ground surface inclination (slope) exceeds 0.2%. It should be noted that the inclination of the ground surface deformation profile ($B$) is insignificant along the ground level except for the zones in the vicinity of the shear band locations that are associated with peak values (Fig. 5a). The inclinations are low at $U$ = 0.05%H and afterwards they start to increase in a steep manner at the shear band locations.

Figure 5b shows the increase of the normalized length of the distorted zone and the location of the center of the distorted zone with increasing vertical bedrock displacement $U$. The center of the distorted zone ($C$) is defined as the horizontal distance between the fault center and the midpoint of the distorted zone. At low bedrock displacements, the length of the distorted zone is negligible. With the formation of the primary shear band, the length of the distorted zone increases to a value of 0.3H at $U$ = 0.085%H, with the center of the distorted zone being located at 0.6H on the side of the primary shear band. With the formation of the secondary shear band and the associated graben, the length of the distorted zone increases to 1.3H, and the center of the distorted zone drifts toward the fault center. Beyond that stage, the length and the center of the distorted zone vary at a slow rate, with the length showing a slight increase in an almost steady manner to a value of 1.53H at $U$ = 10%H, and the center of the distorted zone drifting slightly toward the fault center to a location of − 0.05H.

## Effect of relative density

The results presented in section 3.1 pertain to the case of fault propagation through dense sands. To investigate the effect of relative density on the fault propagation mechanism, the

**Fig. 4** Shear band formation at different vertical bedrock displacements ($U$ = **a** 0.01, **b** 0.014, **c** 0.015, and **d** 0.2 m for the reference model (dense sand, dip angle = 45°, soil layer thickness $H$ = 20 m)

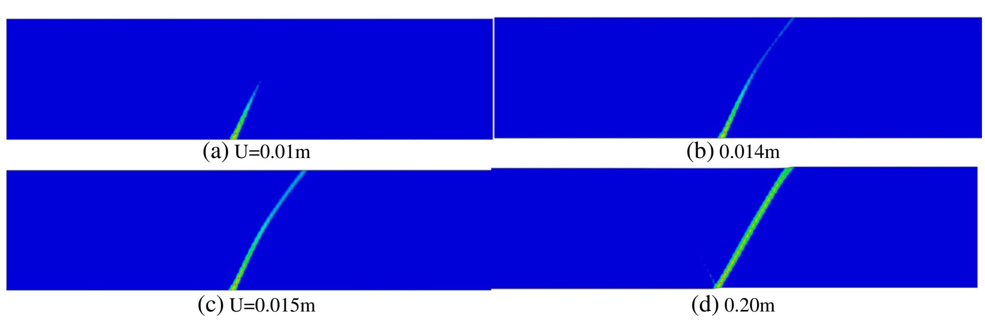

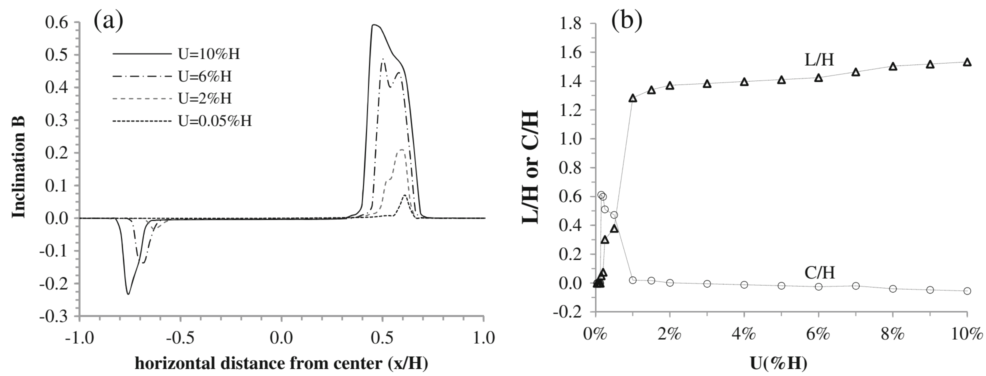


**Fig. 5** For various vertical bedrock displacements *U* (%H). **a** Inclination of the ground surface profile and **b** variation of the normalized length (L/H) and center (C/H) of the distorted zone for the case of the reference model (dense sand, dip angle = 45°, soil layer thickness *H* = 20 m)

relative density is varied from RD = 80% to RD = 50% (medium dense sand) and RD = 20% (loose sand). The effect of relative density on the normalized ground surface deformation profiles (*y*/*H*) is illustrated in Fig. 6a for vertical bedrock displacements of *U* = 2, 6, and 10% of the soil layer thickness (*H*). Results indicate that the inclination of the ground deformation profile in the shearing zone is the greatest for dense sands and decreases in the medium dense and loose sand cases, respectively. As a result, the outcrop location of the ground surface profile is the farthest for the loose sand and becomes closer to the center of the fault as the relative density increases. In fact, the distance *S* (see Fig. 6b) increases from about 0.6H for the dense sand case to 0.8H for the medium dense sand case and to 0.9H for the loose sand case. An investigation of the extent of the zone of concentration of plastic strains within the propagating shear band (Fig. 6b) indicates that the shear bands are the widest and farthest for the loose sand case, and become narrower and more inclined as the relative density increases. These results are realistic since plastic strains/deformations are expected to be more localized and concentrated for dense sands which are stiffer and more dilative in nature, compared to loose sands which are softer and amenable to larger contractive volumetric strains during shear band formation.

## Effect of fault dip angle

The fault propagation mechanism is expected to be sensitive to the dip angle of the normal fault in the base rock. Figure 7a, b show the ground surface deformation profiles (*y*/*H*) and the accumulated plastic strains due to fault movement for different values of dip angles (15°, 30°, 45°, 60°, and 75°) at a vertical bedrock displacement *U* = 10%H.

Results on Fig. 7 indicate that shallower dip angles increase the likelihood of the formation of graben structures as the fault propagates upward through the sand layer. These grabens decrease in length for steeper dip angles up to a dip angle of 60° where only one primary shear band forms. For the steepest dip angle of 75°, multiple secondary shear bands form on both sides of the fault, resulting in a multi-step deformation profile on the ground surface.

By comparing the curves on Figs 6 and 7, it is noticed that the ground surface deformation profile and the shear bands locations are more influenced by the dip angle than the relative

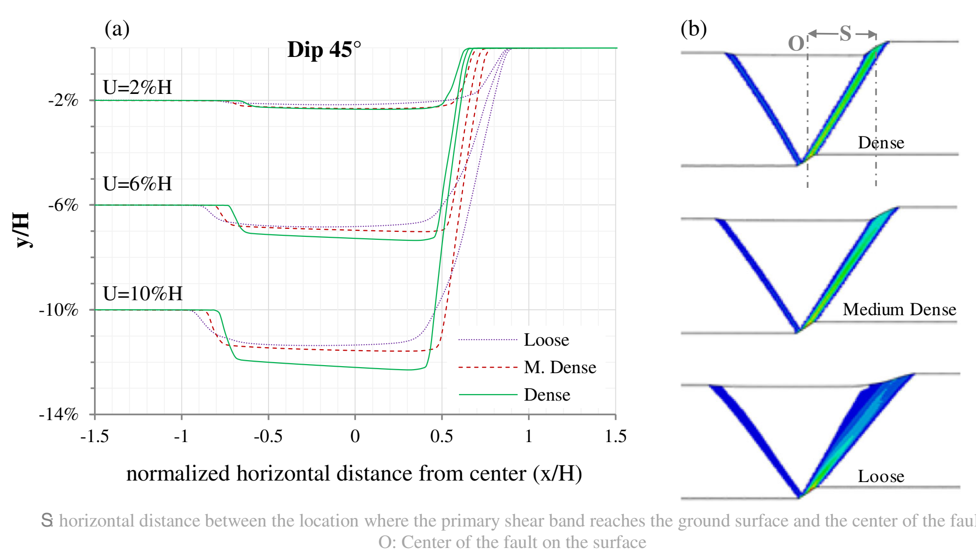


**Fig. 6** For normal faulting dipping at 45° for cases of dense, medium dense, and loose sand. **a** Ground surface deformation profiles (*y*/*H*) for vertical bedrock displacements *U* = 2, 6, and 10%H. **b** Spatial variation of plastic strains within the shear bands at *U* = 10%H

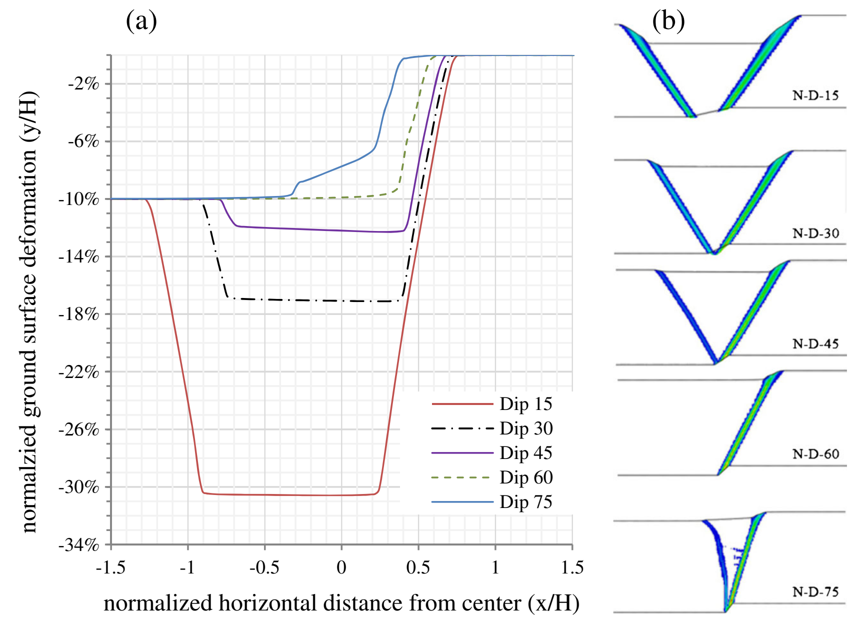


**Fig. 7** Seabed dense sand layer of thickness $H = 20$ m subjected to normal fault of dip angles 15°, 30°, 45°, 60°, and 75° at a vertical bedrock displacement $U = 10\%$H. **a** Normalized ground surface deformation profiles. **b** Spatial variation of plastic strains within the shear bands

density. For the ground surface deformation profiles, the outcrop locations are farthest from the center of the fault for the shallowest dip angle of 15° ($S$ = 0.75H) and closest for the steepest dip angle of 75° ($S$ = 0.4H). The length of the graben is largest for a dip angle of 15° as it attains a length of $L_g$ = 1.5H and a scarp height of $s_g$ = 20.5%H on the hanging wall side at $U$ = 10%H. The length and scarp of the graben decrease with increasing dip angle to attain a length of $L_g$ = 1.45H and scarp height = 2.3%H for a dip angle of 45°. Beyond this dip angle of 45°, a graben does not form.

## Combined effect of relative density and dip angle

### *Extent and location of the shear surface/band*

The predefined location of the shear band with respect to the fault center (denoted by "S") was normalized by the soil thickness "H" and plotted on Fig. 8a for all the cases analyzed. The results are presented for a normalized fault displacement of 2.75%H to allow for comparison with results of fault propagation from previous published studies (Loukidis et al. 2009 and Anastasopoulos et al. 2008).

Results on Fig. 8a indicate that the normalized locations of the primary shear bands of normal faults seem to be sensitive to the sand relative density and to the dip angle. The distance to the shear band is farthest for the loose sand case as the corresponding values range from $S$ = 0.62H at a steep dip angle of 75° to values of 0.78H at a dip angle of 15°. For the shallowest dip angle of 15°, $S$ decreases from a value of 0.78H to 0.59H as the sand relative density is changed from loose to dense. Loose sand is characterized by lower strength and stiffness properties that allow the shear band to extend over a larger distance. The distance to the shear band $S$ for cases with different relative densities differs by a range of 0.1H to 0.2H. As the dip angle of the fault increases, the normalized distance to the shear band is found to slightly decrease, irrespective of the sand relative density. From a dip angle of 15° to 75°, $S$ decreases in a parabolic manner to lose

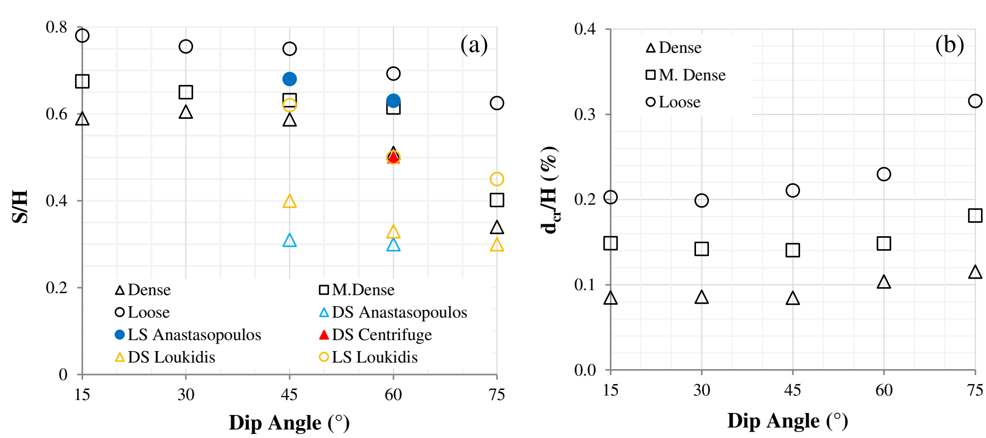


**Fig. 8** Variation of **a** normalized primary shear band locations at a vertical bedrock displacement $U = 2.75\%$H compared with previous researchers and **b** normalized critical fault displacements versus the fault dip angle (15°, 30°, 45°, 60°, and 75°)

almost half of its value from 0.755H to 0.42H for loose sand and 0.6H to 0.3H for dense sand. The decrease in $S$ for steeper fault angles is expected given that smaller values of $S$ are indicative of steeper shear bands which go hand in hand with steeper dip angles.

A comparison between the results presented in Fig. 8 and similar published results indicate that the published normalized shear band locations for cases with loose sands are in the range of values obtained in our study. The same applies to the centrifuge tests that were conducted with dense sands. For the case of published numerical studies involving dense sands, results on Fig. 8a indicate differences with the results of our study, with the published results showing normalized shear band locations that are consistently smaller than our results. The difference in the results between our model and other published models is expected to be associated with how the soil parameters were defined in the finite element analysis. In our study, all soil properties (modulus of elasticity, dilation angle, and friction angle) were assumed to vary with depth to provide a realistic model of soil behavior for granular materials that are dependent on confining pressure. A sensitivity study done by the authors demonstrated that the stiffness, dilation angle, and the friction angle of the sand are critical factors that govern the fault propagation mechanism and shear band formation.

The variation of the normalized critical bedrock displacement ($d_{cr}/H$) that is required for the shear band to propagate to the ground surface is plotted in Fig. 8b as a function of the dip angle of the normal fault for dense, medium dense, and loose sand cases. Results indicate that the required bedrock displacement for the rupture to reach the surface is relatively small (< 0.4%H), with minor variations for different fault dip angles (difference in the order of 0.03%H) except for the case of a dip angle of 75° where maximum differences in the order of 0.13%H are observed in $d_{cr}$/H for the case of loose sands. This can be explained by the fact that larger dip angles require a larger inclined bedrock displacement for the shear band to propagate to the surface. The higher bedrock displacements that are required for the shear bands to reach the surface in loose sands could be attributed to the formation of wider and multiple shear bands that require larger fault displacements to force the fault rupture to propagate to the surface.

*Length and Center of Distorted Zone*

The numerical results are analyzed to determine the length ($L$) and center ($C$) of the distorted zone normalized with respect to the soil layer thickness $H$. The normalized values of $L$ and $C$ are plotted as a function of the fault dip angle for all the analyzed cases at a vertical bedrock displacement of 10% of the soil layer thickness $H$ (Fig. 9). Results on Fig. 9 indicate that the normalized length of the distorted zone for normal faults is more affected by the dip angle of the fault than it is affected by the density of the soil. The range of the difference in the length of the distorted zone between the dense sand cases and the loose sand cases is 0.3H–0.4H which is relatively low.

For a normal fault with a dip angle of 15°, $L/H$ ranges from about 2.1 to 2.4 for the loose and dense sand cases, respectively. These numbers decrease for steeper dip angles, reaching values as low as 0.9 to 1.3 for dense and loose sand cases with a steep fault dip angle of 60°. The larger values of $L/H$ for lower dip angles (15°, 30°, and 45°) are related to the formation of graben structures which magnify the length of the distorted zone by a factor of about 2.0 compared to the cases where these structures do not form. The secondary shear bands which form in the opposite direction to the primary shear band propagate to the surface and shift the location of the center of the distorted zone toward the center O.

As the dip angle increases, the distance to the shear bands decreases and therefore the length of the distorted zone decreases. It is noticed that the centers of the distorted zones for the cases where grabens form coincide for sands of different

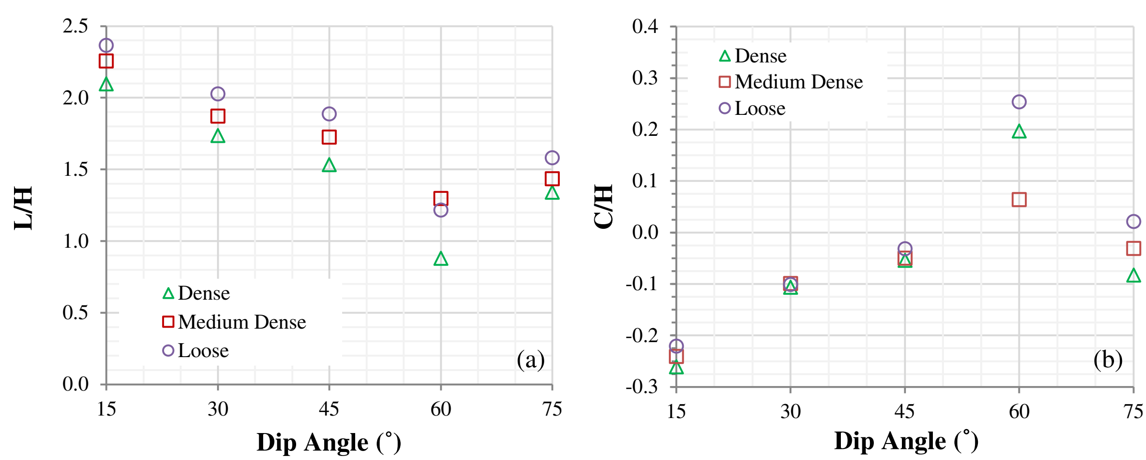


**Fig. 9** Normalized length (L/H) and center of the distorted zone (C/H) versus the normal fault dip angle (15°, 30°, 45°, 60°, and 75°) for cases of dense, medium dense, and loose sand at a vertical bedrock displacement $U$ = 10%H ($H$ = 20 m)

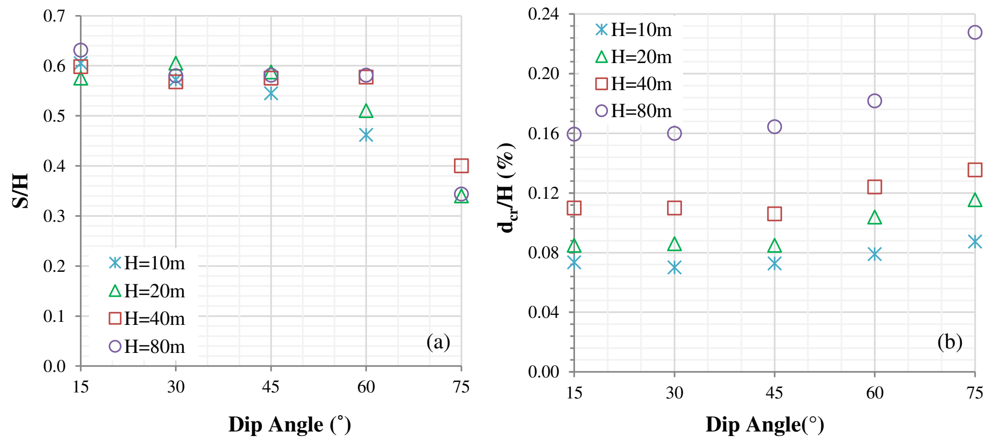


**Fig. 10** For different dense sand layer thicknesses $H$ = 10, 20, 40, and 80 m subjected to normal faults of dip angles 15°, 30°, 45°, 60°, and 75°. **a** Normalized shear band locations (S/H) at $U$ = 2.75%H and **b** normalized critical bedrock displacements ($d_{cr}$/H%)

relative densities. For the dip angle of 60°, only one primary shear band forms, and the center of the distorted zone is located on the footwall side. As the dip angle is increased beyond 60° (dip angle of 75°), L/H increases from 0.88 and 1.3 for dense and loose sand, respectively, to 1.34 and 1.58 at a dip angle of 75°. The 75° dip angle case is associated with the formation of secondary shear bands on the hanging wall side. These secondary bands increase the length of the distorted zone and shift its center toward that hanging wall side to C/H = − 0.1 and 0 for dense and loose sand, respectively.

### Effect of thickness of overlying sand layer

Since the majority of the results of the previous sections were presented in a normalized form (normalized with respect to the height of the overlying sand layer), it is important to investigate whether the results of the fault propagation analysis remain valid for different soil overburden heights. For this purpose, the finite element analyses that were conducted in the previous sections with a soil height of 20 m were repeated for cases involving soil thicknesses H of 10, 40, and 80 m.

An investigation of the sensitivity of the normalized ground surface deformation profiles to the height of the overlying sand layer (not presented for length limitations) leads to the conclusion that the normalized ground surface deformation profiles are relatively insensitive to the thickness of the sand layer, particularly for smaller dip angles (15°, 30°, and 45°). A comparison between the normalized shear band locations for different sand layer thicknesses (Fig. 10a) indicates that the normalized locations of the shear bands are not sensitive to the soil layer thickness. The shear band locations are relatively similar with maximum differences in the order of 0.1H (for dip angle of 60°). These minor differences are attributed to the fact that the soil properties that govern the propagation mechanism depend on depth. This may affect the process of shear band formation leading to small variations in the resulting shear bands in layers of different thicknesses.

On the other hand, the normalized critical inclined bedrock displacements ($d_{cr}$/H) that are required for the shear band to reach the surface seem to be highly sensitive to the sand layer thickness as indicated in Fig. 10b. Results show that the normalized critical bedrock displacement is larger for larger soil layer thicknessess. The difference between the critical bedrock displacements increases with the sand layer thickness and the dip angle in a non-linear manner. This indicates that normalizing the required displacement by the height of the overburden soil is not associated with a constant $d_{cr}$/H value for the different case scenarios investigated. The lack of normalization is explained by the fact that soils at larger depths exhibit higher stiffness and lower peak friction and dilation angles since the soils are more confined and constrained. As a result, a higher bedrock displacement is required for the shear bands to reach the surface. It could be concluded that for the cases involving normal faults, the thickness of the overlying soil plays a role in defining the bedrock displacements that are required for the fault to physically propagate to the surface. In fact, the required normalized bedrock displacements for a sand thickness of 80 m is almost double to triple that of the displacements required for a sand thickness of 10 m (see Fig. 10b).

## Conclusions

In this paper, a comprehensive investigation of the mechanism of fault propagation in offshore sand deposits that overly dip-slip normal faults is conducted. The investigation was conducted using the finite element method with a model consisting of a sand layer that is modeled using the Modified Mohr Coulomb constitutive model that is capable of modeling strain softening. The cases considered included different cases of sand relative density, fault dip angle, and sand layer thickness. The soil strength and stiffness properties were modeled to vary with depth to incorporate the effect of confinement on the fault propagation mechanism. Based on the results, the following can be concluded:

- The normalized ground surface deformation profiles for normal faults are more sensitive to the dip angle than the relative density.
- Grabens are more likely to form with normal faults having shallow dip angles. The width of the graben is larger for cases with small dip angles.
- The primary shear band locations are farther from the center of the fault for loose sands and smaller fault dip angles and vary slightly between the different soil layer thicknesses.
- The shear band reaches the top surface at small values of bedrock displacement. The normalized bedrock displacement required for the rupture to reach the surface is slightly larger for lower relative densities, shallower dip angles, and larger soil layer thicknesses.
- The dip angle is a more critical factor to the length of the distorted zone compared to the relative density. Cases that include graben formation show distorted zones with lengths that are twice the lengths for cases where only a primary failure plane forms. In the former, the center of the distorted zone is shifted toward the center of the fault. The normalized length of the distorted zone is slightly larger for cases of lower relative densities.
- Except for the normalized critical bedrock displacement, the results of the fault propagation study for normal faults could be presented in normalized format since the normalized results are relatively insensitive to the height of the overlying soil layer.

The findings and conclusions presented above cover a wide range of cases and are of direct relevance to the design of pipelines that are supported on sand deposits overlying normal dip-slip faults. For any combination of design fault displacement, sand layer thickness, and sand relative density, the charts could be used to predict the location and extent of the distorted zone that will be affected by the fault propagation process. Since the thickness of the sand layer could vary laterally across the fault plane/zone that is crossed by pipelines, there is a need for estimating the location and extent of the distorted zone for different values of normalized fault displacement, since each value represents a combination between the anticipated fault displacement and the potential sand layer thickness at the locations where the pipeline crosses the laterally varying fault plane. As a result, a comprehensive and reliable site investigation should be designed and executed to allow for (1) establishing realistic stratigraphic sections that show the variability in the thickness of a cohesionless sand cover in reference to the location of the faulted basement bedrock and (2) determining the soil properties of the cover layer (with particular emphasis on the relative density) and any expected spatial variability that might govern the uncertainty in the relevant soil properties that may affect the analysis.

**Acknowledgements** The authors would like to acknowledge the support of the Lebanese National Council for Scientific Research and the University Research Board of the American University of Beirut for supporting this research.

## References

ABAQUS, Inc. (2013) ABAQUS V.6.13 user's manual, providence, R.I

Abers GA (1991) Possible seismogenic shallow-dipping normal faults in the Woodlark-D'Entrecasteaux extensional province, Papua New Guinea. Geology 19(12):1205–1208. https://doi.org/10.1130/00917613(1991)019<1205:PSSDNF>2.3.CO;2

Anastasopoulos I, Gazetas G, Bransby MF, Davies MCR, El Nahas A (2007) Fault rupture propagation through sand: finite element analysis and validation through centrifuge experiments. J Geotech Geoenviron ASCE, 133(8):943–958. https://doi.org/10.1061/(ASCE)1090-0241(2007)133:8(943)

Belousov VV (1961) Experimental geology. Sci Am 204(2):96–107

Bendimerad F, Johnson L, Coburn A, Rahnama M, Morrow G (2000). Event report, Kocaeli, Turkey earthquake. RMS reconnaissance team

Bolton MD (1986) The strength and dilatancy of sands. Geotechnique 36(1):65–78. https://doi.org/10.1680/geot.1986.36.1.65

Bransby MF, Davies MCR, El Nahas A (2008a) Centrifuge modelling of normal fault-footing interaction. Bull Earthq Eng, 6 (4 ):585–605. https://doi.org/10.1007/s10518-008-9079-0

Bransby MF, Davies MCR, El Nahas A, Nagaoka S (2008b) Centrifuge modelling of reverse fault-foundation interaction. Bull Earthq Eng, 6 (4 ):607–628. https://doi.org/10.1007/s10518-008-9080-7

Bray JD, Seed RB, Seed HB (1993) 1 g small-scale modelling of saturated cohesive soils. Testing J American Society for Testing and Materials 16(1):46–53. https://doi.org/10.1520/GTJ10266J

Bray JD, Seed RB, Seed HB (1994) Analysis of earthquake fault rupture propagation through cohesive soil. J Geotech Eng ASCE 120(3): 562–580. https://doi.org/10.1061/(ASCE)0733-9410(1994)120:3(562)

Chang YY, Lee CJ, Huang WC, Hung WY, Huang WJ, Lin ML, Chen YH (2015) Evolution of the surface deformation profile and subsurface distortion zone during reverse faulting through overburden sand. Eng Geol 184:52–70. https://doi.org/10.1016/j.enggeo.2014.10.023

Cole DA Jr, Lade PV (1984) Influence zones in alluvium over dip-slip faults. J Geotech Eng ASCE 110(5):599–615. https://doi.org/10.1061/(ASCE)0733-9410(1984)110:5(599)

Emmons RC (1969) Strike-slip rupture patterns in sand models. Tectonophysics 7(1):71–87. https://doi.org/10.1016/0040-1951(69)90065-1

Horsfield WT (1977) An experimental approach to basement-controlled faulting. Geologie En Mijnbouw, Haarlem, The Netherlands, 56(4): 363–370

Johansson J, Konagai K (2004) Fault surface rupture experiments: a comparison of dry and saturated soils. In Proceeding of 27th Symposium on Earthquake Engineering, JSCE, Paper (No. 271)

Kelson KI, Kang KH, Page WD, Lee CT, Cluff LS (2001) Representative styles of deformation along the Chelungpu fault from the 1999 Chi-Chi (Taiwan) earthquake: geomorphic characteristics and responses of man-made structures. Bull Seismol Soc Am 91(5):930–952. https://doi.org/10.1785/0120000741

Koerner RM (1970) Effect of particle characteristics on soil strength. Journal of Soil Mechanics & Foundations Div

Kulhawy FH, Mayne PW, (1990) Manual on estimating soil properties for foundation design. Ithaka, New York, Cornell University, EPRI EL-6800

Lade PV, Cole DA Jr, Cummings D (1984) Multiple failure surfaces over dip-slip faults. J Geotech Eng ASCE 110(5):616–627. https://doi.org/10.1061/(ASCE)0733-9410(1984)110:5(616)

Lin ML, Chung CF, Jeng FS (2006) Deformation of overburden soil induced by thrust fault slip. Eng Geol 88(1):70–89. https://doi.org/10.1016/j.enggeo.2006.08.004

Loukidis D (1999) Active fault propagation through soil. Dissertation, National Technical University, Athens

Loukidis D, Bouckovalas GD, Papadimitriou AG (2009) Analysis of fault rupture propagation through uniform soil cover. J Soil Dyn Earthq Engrg 29(11):1389–1404. https://doi.org/10.1016/j.soildyn.2009.04.003

Nakai T, Muir Wood D, Stone KJL (1995) Numerical calculations of soil response over a displacing basement. Soils Found 35(2):25–35. https://doi.org/10.3208/sandf1972.35.2_25

Nollet S, Vennekate GJ, Giese S, Vrolijk P, Urai JL, Ziegler M (2012) Localization patterns in sandbox-scale numerical experiments above a normal fault in basement. J Struct Geol 39:199–209. https://doi.org/10.1016/j.jsg.2012.02.011

Rietbrock A, Tiberi C, Scherbaum F, Lyon-Caen H (1996) Seismic slip on a low angle normal fault in the Gulf of Corinth: evidence from high-resolution cluster analysis of microearthquakes. Geophys Res Lett 23(14):1817–1820

Roth WH, Sweet J, Goodman RE (1982) Numerical and physical modelling of flexural slip phenomena and potential for fault movement. Rock Mech (Suppl 12):27–46. https://doi.org/10.1007/978–3–7091-8665-7_3

Sanford AR (1959) Analytical and experimental study of simple geologic structures. Geol Soc of Am Bull 70(Jan.):19–52. https://doi.org/10.1130/0016-7606(1959)70[19:AAESOS]2.0.CO;2

Scott RF, Schoustra JJ (1974) Nuclear power plant siting on deep alluvium. Journal of the Geotechnical Engineering Division ASCE 100(GT4):449–459

Scott RF, (1987) Failure. Geotechnique, London, England, 37(4): 423–466

Schanz T, Vermeer PA (1998) On the stiffness of sands. Géotechnique 48: 383–387

Taniyama H, Watanabe H (2002) Deformation of sandy deposits by reverse faulting. Struct Eng/Earthquake Eng JSCE 19(2):209–219. https://doi.org/10.2208/jsceseee.19.209s

Trimintziou M, Sakellariou M, Psarropoulos P (2015) Designing offshore pipelines facing the geohazard of active seismic faults. World Academy of Science, Engineering and Technology, International Journal of Civil, Environmental, Structural, Construction and Architectural Engineering, 9(6): 775–784

White RJ, Stone KJL, Jewel RJ (1994) Effect of particle size on localization development in model tests on sand. In: Leung, lee, tan (eds) centrifuge 94. Balkema, Rotterdam, pp 817–822